Available online at www.sciencedirect.com

ScienceDirect

Acta Materialia 78 (2014) 78–85

Acta MATERIALIA

www.elsevier.com/locate/actamat

Elemental partitioning and mechanical properties of Ti- and Ta-containing Co–Al–W-base superalloys studied by atom probe tomography and nanoindentation

Ivan Povstugar [a], Pyuck-Pa Choi [a,*], Steffen Neumeier [b], Alexander Bauer [b], Christopher H. Zenk [b], Mathias Göken [b], Dierk Raabe [a]

[a] Department of Microstructure Physics and Alloy Design, Max-Planck-Institut für Eisenforschung, Max-Planck-Str. 1, 40237 Düsseldorf, Germany
[b] Friedrich-Alexander-Universität Erlangen-Nürnberg (FAU), Materials Science & Engineering, Institute I, Martensstr. 5, 91058 Erlangen, Germany

Received 17 March 2014; received in revised form 3 June 2014; accepted 9 June 2014
Available online 16 July 2014

Abstract

Elemental partitioning and hardness in Ti- and Ta-containing Co-base superalloys, strengthened by γ'-Co_3(Al, W) precipitates, have been studied by local measurements. Using atom probe tomography, we detect strong partitioning of W (partitioning coefficients from 2.4 to 3.4) and only slight partitioning of Al (partitioning coefficients $\leqslant$1.1) to the γ'-Co_3(Al, W) phase. Al segregates to the γ/γ' phase boundaries, whereas W is depleted at the γ side of the boundaries after aging at 900 °C and slow air cooling. This kind of Al segregation and W depletion is much less pronounced when water quenching is applied. As a result, these effects are considered to be absent at high temperatures and therefore should not influence the creep properties. Ti and Ta additions are found to strongly partition to the γ' phase and greatly increase the γ' volume fraction. Our results indicate that the alloying elements Al, W, Ti and Ta all occupy the B sublattice of the A_3B structure ($L1_2$ type) and affect the partitioning behavior of each other. Nanoindentation measurements show that Ta also increases the hardness of the γ' phase, while the hardness of the γ channels remains nearly constant in all alloys. The change in hardness of the γ' phase can be ascribed to the substitution of Al and W atoms by Ti and/or Ta.

Keywords: Cobalt-base superalloys; Atom probe tomography (APT); Nanoindentation

1. Introduction

Ni-base superalloys are nowadays the key engineering materials for high-temperature parts in aircraft engines and stationary turbines for power generation. The excellent creep resistance of these alloys is provided by a microstructure consisting of coherent cuboidal γ' ($L1_2$) precipitates dispersed in a γ (face-centered cubic (fcc)) matrix. Since the recent discovery of the ternary γ'-Co_3(Al, W) intermetallic phase by Sato et al. [1], Co-base superalloys with a similar type of γ/γ' microstructure have emerged as a promising alternative to Ni-based alloys, with a potential to exhibit even better properties. In particular, Co–Al–W-based alloys may be less prone to freckling formation [2] and possess higher melting temperatures than Ni-based superalloys [3,4], but they still exhibit lower creep resistance, mainly due to a lower γ' solvus temperature. In order to compete with their Ni-based counterparts and to achieve commercialization, various properties of γ'-strengthened Co-based superalloys must be further understood and optimized. Knowledge-based alloy design is necessary to optimize the thermal stability, γ/γ' lattice misfit, volume fraction of the γ'phase and thus the mechanical properties at elevated operating temperatures.

* Corresponding author. Tel.: +49 211 6792 167; fax: +49 211 6792 333.
E-mail address: p.choi@mpie.de (P.-P. Choi).

http://dx.doi.org/10.1016/j.actamat.2014.06.020
1359-6454/

Among various alloying elements for Co–Al–W-based superalloys, Ti and Ta are of special interest as they are known to increase the solvus temperature, phase stability, and volume fraction of γ' [3–5]. Adding about 2 at.% Ti to a ternary Co–Al–W alloy raises the γ' solvus temperature by >90 °C and the γ' volume fraction by ~20% [4,6]. Similar effects are observed upon alloying with Ta. Moreover, small additions of Ta (~2 at.%) are reported to enhance the yield strength of the Co–9Al–9W alloy, in particular at temperatures above 700 °C [3,7]. On the other hand, exceedingly high amounts of Ti and Ta promote the formation of deleterious phases such as Co_2AlTi or Co_3W [5,8], which are not coherent with the γ matrix and deteriorate the high-temperature properties.

Recently, atom probe tomography (APT) was applied to study elemental partitioning and γ' coarsening in ternary Co–Al–W and a few quaternary systems [9–11]. However, systematic studies of the influence of alloying elements on elemental partitioning at the nanometer scale and their respective effects on the mechanical properties have not been carried out so far. Quantitative analyses of γ/γ' compositions were performed for several quaternary systems using electron probe microanalysis [6] or energy dispersive X-ray spectroscopy [12], but the spatial resolution of these techniques is usually limited to a few tens of nanometers. Consequently, the composition of nanoscale features such as the γ channels remains questionable when measured using these techniques. Here, we report on the analysis of phase compositions and elemental distributions within the two-phase γ/γ' microstructure of Co–Al–W–(Ti/Ta) alloys by means of APT. Changes in microstructure and volume fraction of γ' upon alloying with Ta and Ti are discussed on the basis of the measured elemental partitioning. The effect of alloying on the hardness of the γ and γ' phases is studied by nanoindentation using an atomic force microscope (NI-AFM), which has been demonstrated to be a valuable tool for measuring solid-solution hardening effects of alloying elements in superalloys [13,14].

2. Experimental details

A systematic composition matrix consisting of four polycrystalline alloys with nominal compositions of Co–9Al–9W (referred to as "ternary"), Co–9Al–9W–2Ti (referred to as "+2Ti"), Co–9Al–9W–2Ta (referred to as "+2Ta") and Co–8Al–9W–2Ti–2Ta (referred to as "+2Ti+2Ta") was investigated, where the numbers denote concentrations of the corresponding alloying elements in at.%. Small amounts of boron (maximum 0.12 at.%) were added to the first three alloys to improve the grain boundary strength.

Ingots of 100 g were prepared by vacuum arc melting, homogenized at 1300 °C for 12 h in an argon atmosphere and subsequently aged at 900 °C for 200 h. All alloys were cooled in air after the heat treatment unless otherwise stated. The deviation from the nominal compositions due to the high melting point of W and evaporation of Al during arc melting did not exceed 0.8 at.% for Al and 0.4 at.% for W, as measured by an Oxford Instruments energy-dispersive X-ray spectroscopy system in a Zeiss Crossbeam 1540 EsB focused-ion-beam (FIB) microscope.

The resulting γ/γ' microstructure was characterized by atomic force microscopy (AFM) and scanning electron microscopy (SEM). The samples were mechanically polished and, in the case of SEM samples, etched for <30 s at room temperature using Vogel's Spar solution (100 ml distilled water, 100 ml 32% HCl, 10 ml 65% HNO_3 and 0.3 ml Dr. Vogel's Spar etchant consisting of 30–50% 1-methoxy-2-propanol and 2.5–5% thiocarbamide).

APT specimens were prepared using a dual-beam FIB system (FEI Helios Nanolab 600) by the conventional lift-out technique described in Ref. [15]. To minimize implantation of Ga ions, a low-energy (5 keV) Ga beam was used for final shaping of the APT tips. APT analyses were done using a reflectron-equipped local electrode atom probe (LEAP™ 3000X HR, Cameca Instruments) in pulsed laser mode. Laser pulses of 532 nm wavelength, 12 ps pulse length, 0.4 nJ energy and 100 kHz frequency were applied, while the base temperature of samples was kept at ~40 K. Data reconstruction and analysis was performed using the Cameca IVAS™ 3.6.6. software package. The first subset of ~1 mio. collected ions was discarded from the data analysis to exclude Ga ions implanted during FIB milling.

The hardness of the γ' precipitates and the γ channels were measured independently using a Triboscope nanoindenter from Hysitron with a cube corner tip installed on a multimode atomic force microscope from Veeco. Samples for nanoindentation were heat treated at 900 °C for 1000 h in order to obtain a coarsened γ/γ' microstructure and to enable separate indentation on both the γ and γ' phases. The samples were ground, subsequently polished with a diamond suspension and additionally chemomechanically polished with a nanodisperse SiO_2 suspension. Two sets of indentation experiments were performed with maximum applied loads of 150 and 250 μN. In previous works [13,14] we showed that for a maximum load of 250 μN the properties of both phases can be determined separately. The alloys investigated in this work, however, still have rather small (265–345 nm) precipitate sizes even after relatively long-term (1000 h) aging. Therefore, nanoindentation tests at a maximum applied load of 150 μN were additionally performed in order to guarantee that the plastic zone under an indent is small enough compared to the precipitate size. The hardness of γ and γ' was determined by analyzing the load–displacement curves recorded during indentation according to the Oliver–Pharr method [16].

3. Results and discussion

3.1. Microstructure of the alloys

After the aging treatment, a two-phase γ/γ' microstructure (similar to that in Ni-based superalloys) is formed. A regular arrangement of well-defined cuboidal γ' particles is clearly visible in the SEM images (Fig. 1), indicating a

small γ/γ' lattice misfit and coherent interfaces. No other phases, such as Co_3W or CoAl, were observed. Both alloying elements, i.e. Ti and Ta, added at the expense of Co, lead to a significant increase in γ' volume fraction in agreement with previous reports [3–5]. When added together, these two elements result in a microstructure where γ streaks become very thin. As a result, necking between adjacent γ' cuboids arises. The precipitate corners become less rounded, indicating an increase in coherency strain at the phase boundaries. The boron-containing alloys exhibit a large number of boride precipitates at the grain boundaries (not shown here; for more details on the GB microstructure we refer to an earlier paper [4]).

3.2. Elemental partitioning between γ and γ'

Fig. 2 shows a three-dimensional elemental map and a concentration profile across the γ/γ' interface, acquired from an APT analysis of the ternary alloy. The data reveal that W atoms clearly partition to the γ' phase, whereas Al partitioning is very low, in agreement with recent studies [9,11]. The partitioning can be quantified in terms of the coefficient K for an element X:

$$K_x = C_x^{\gamma'}/C_x^{\gamma}, \tag{1}$$

where $C_x^{\gamma'}$ and C_x^{γ} are the concentrations of the element X in γ' and γ, respectively. The phase compositions were accurately measured in subvolumes containing at least 1 mio. ions and located at least 5 nm away from the phase boundaries. The compositions and the associated partitioning coefficients are given in Table 1. The observed partitioning behavior of Al and W is very different from that of

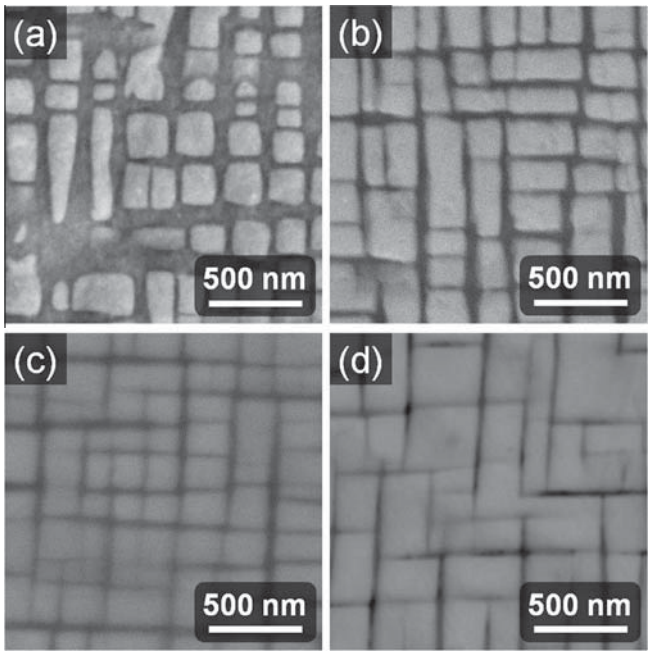

Fig. 1. SEM images of the microstructure after aging in (a) ternary Co–9Al–9W, (b) +2Ti, (c) +2Ta, (d) +2Ti+2Ta alloys.

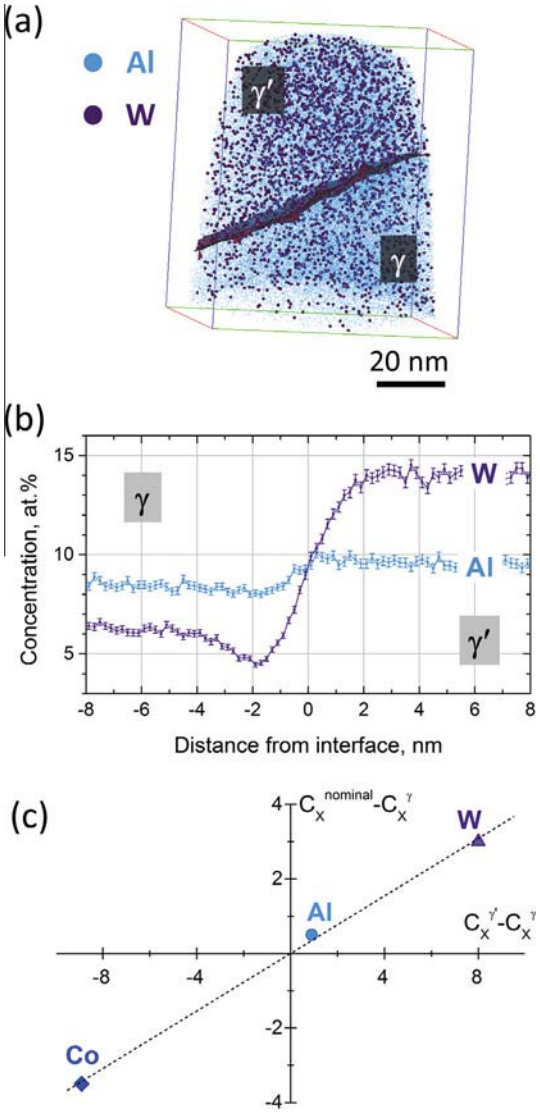

Fig. 2. (a) APT atom map, (b) elemental concentration profiles and (c) lever rule plot used for calculation of the γ' volume fraction for the aged ternary Co–9Al–9W alloy.

Ni-based superalloys, where Al strongly partitions to the γ' phase ($K_{Al} > 5$), while W typically shows a low partitioning tendency ($K_W < 2$) [17,18].

If the individual phase compositions are known, the mole fractions of γ and γ' phases can be calculated using the lever rule based on the mass balance equation:

$$C_x^{\gamma}(1 - f_{\gamma'}) + C_x^{\gamma'} \cdot f_{\gamma'} = C_x^{\text{nominal}}, \tag{2}$$

where $f_{\gamma'}$ is the γ' mole fraction, C_x^{γ} and $C_x^{\gamma'}$ are the concentrations of an element X in the corresponding phases (measured by APT), and C_x^{nominal} is the nominal concentration of X in the alloy. When Eq. (2) is rewritten as:

$$f_{\gamma'} = \left(C_x^{\text{nominal}} - C_x^{\gamma}\right) / \left(C_x^{\gamma'} - C_x^{\gamma}\right),$$

and the values for different alloying elements are plotted on a graph, a linear regression analysis can be used to minimize the influence of errors in measured concentrations

Table 1
Phase compositions, partitioning coefficients (K_x) and γ' volume fraction.

Alloy	$\gamma\|\gamma'$ Composition, at.%					Partitioning coefficients				γ' Volume fraction, %
	Co	Al	W	Ti	Ta	Al	W	Ti	Ta	
Ternary	85.5|76.6	8.5|9.4	6.0|14.0	–	–	1.1	2.6	–	–	38 ± 2
+2Ti	85.0|76.4	8.8|8.8	5.0|12.1	1.0|2.6	–	1.0	2.4	2.5	–	57 ± 1
+2Ta	85.0|75.5	9.0|8.9	4.5|12.0	–	0.55|2.9	1.0	2.7	–	5.3	56 ± 1
+2Ti+2Ta	87.4|75.9	8.1|8.5	3.4|11.8	0.7|2.3	0.27|2.2	1.0	3.4	3.3	8.1	76 ± 2

(see Fig. 2c). This approach gives the mole fractions of phases directly equal to their volume fractions in the studied case, since the difference in atomic densities of γ and γ' is negligible. Applied to the ternary Co–9Al–9W alloy, the lever rule gives a γ' volume fraction of 38%.

Ti or Ta added to the Co–Al–W alloy clearly partition to the γ' phase, thus showing a similar trend as in Ni-based alloys (see Table 1). Among these two elements, Ta has a higher tendency to partition to the γ' phase. The degree of W partitioning remains almost unaffected in the +2Ti and +2Ta alloys, while partitioning of Al completely disappears. The γ' volume fraction calculated by the lever rule rises to 56–57% for both +2Ti and +2Ta alloys.

In the +2Ti+2Ta alloy, i.e. when Ti and Ta are added together, both elements show even stronger partitioning to the γ' phase (Fig. 3). The partitioning of W slightly increases as well, whereas virtually no partitioning of Al is found. The γ' volume fraction reaches 76%, i.e. doubles with respect to the ternary alloy, although only 4 at.% of Co was substituted by Ti and Ta together. This result indicates that Ti and Ta have a more pronounced effect on the formation of the γ' phase than Al or W. Another positive influence of these elements is an increase in the γ' solvus temperature of the corresponding alloys [4]. Based on these results it can be concluded that Ti and Ta are likely to act as γ' stabilizers.

3.3. Lattice site occupancy in the γ' ($L1_2$) phase

The compositional analysis shows that the Co concentration in the γ' phase is 75–76 at.% in all analyzed alloys, while the concentration sum of the remaining alloying elements (Al, W, Ti and Ta) is close to 24–25 at.%. This result is consistent with occupation by Al, W, Ti and Ta atoms of the B sublattice in the A_3B ($L1_2$-type) intermetallic compound, i.e. the same sublattice as occupied by Al atoms in the ordered Ni_3Al compound. Due to the limited spatial resolution of the APT technique in pulsed laser mode and the irregular field evaporation sequence of the detected ions in this alloy, we were not able to resolve individual atomic layers in the APT atom maps.

Table 1 shows that the Co concentration in γ' slightly exceeds the value characteristic for the "nominal" Co_3(Al, W) stoichiometry. This deviation may occur due to anti-site defects, i.e. Al sites substituted with Co atoms, which have been studied by ab initio calculations and

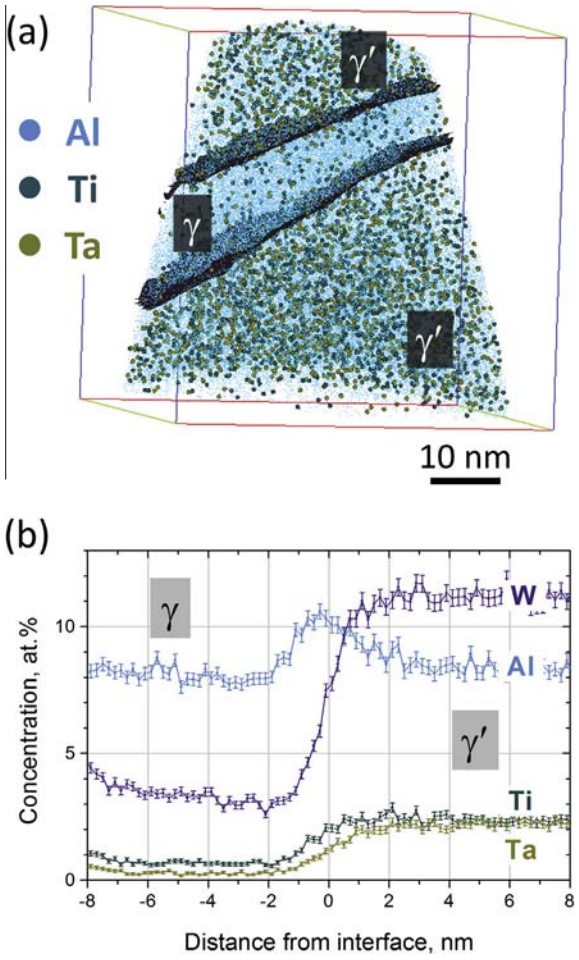

Fig. 3. (a) APT atom map and (b) elemental concentration profiles for the aged +2Ti+2Ta alloy.

reported to be energetically favorable [19]. However, such a concentration deficiency may also easily originate from field evaporation artifacts of APT measurements. The reported measurements were carried out in laser mode, as mentioned in Section 2, since voltage mode measurements resulted in premature fracture of APT specimens. Nevertheless, two small datasets (~0.3 mio. ions each) containing the γ' phase volumes were collected in voltage mode for the Co–9Al–9W alloy. The compositions of the γ' phase acquired from voltage and laser mode measurements are compared in Table 2. The Co concentration in the γ' phase measured in voltage mode is slightly below the "ideal"

75 at.%, whereas laser mode measurements systematically result in an excess of Co by 1–2 at.%. The concentrations of Al and W also depend on the applied probing mode. The difference lies beyond the $\pm 2\sigma$ confidence interval of the error caused by a finite number of atoms in the APT datasets. Preferential evaporation/retention [20], preferential loss of some elemental species due to detector multiple events [21] or uncertainties in ranging of APT mass spectra [22] may account for such relatively small compositional deviations. Hence, the observed small discrepancies between measured and "ideal" compositions for the $L1_2$-type ordered $Co_3(Al, W)$ cannot be considered as a proof of a non-stoichiometry of the γ' phase.

3.4. Compositional variations at γ/γ interfaces

A careful inspection of the elemental concentration profiles across a γ/γ' phase boundary (e.g. Fig. 3) reveals an interesting feature: all analyzed interfaces show a region in the γ phase located just next to the interface, which is depleted of W. The depletion level is 1–2 at.% W and the width of the depletion region is 5–10 nm. Additionally, segregation of Al is observed directly at the interfaces, with an excess of up to 2 at.% compared to the bulk concentration. Since Al and W have atomic radii different from that of Co, such effects may change the local lattice parameters of γ and γ', which, in turn, may influence lattice misfit and dislocation motion across the interface during creep deformation. The observed concentration profiles of Al and W possibly emerge under cooling after heat treatment. The depletion zones, ranging over several nanometers, are indicative of a non-equilibrium state, i.e. they may arise due to limited diffusivity of Al and W during cooling and may not exist at high temperatures (such as operation temperatures of superalloys), when diffusion is fast. To clarify this aspect, the +2Ti alloy sample was additionally prepared by applying water-quenching after aging at 900 °C. The concentration profiles measured by APT for both air-cooled and water-quenched samples are presented in Fig. 4. The W depletion and Al segregation at the γ/γ' interface are much less pronounced, strongly suggesting that these processes occur during slow cooling. They are not entirely suppressed even by water quenching due to a limited quenching rate.

The emergence of the W-depleted zone during cooling can be qualitatively understood by taking into account the binary Co–W phase diagram [23]. According to this, the solubility of W in γ-Co is ~5 at.% at 900 °C and drops with decreasing temperature. A similar trend can be assumed for the alloys studied in this work. This conclusion is supported by the recent APT studies by Meher et al. [10], where a decrease of the bulk W concentration in the γ phase of an Co–Al–W alloy was detected when the aging temperature was lowered from 900 to 800 °C. In the present study, when the alloy is slowly cooled from the aging temperature of 900 °C, excessive W is rejected from the γ phase into the growing γ' precipitate, forming a depleted zone at the γ side of the phase boundary and a pile-up at the γ'-side (see Fig. 4a). The widths of these zones are limited by the mean diffusion length of W. In the case of water-quenching, the time for W diffusion is very short and hence the width of the W depletion zone strongly decreases (see Fig. 4b) as compared to air cooling. Using the standard expression for bulk diffusion:

$$\langle x \rangle = 2\sqrt{D \cdot t}, \tag{3}$$

in conjunction with the diffusion coefficient of W in fcc Co of $D = 3 \cdot 10^{-18}$ m^2 s^{-1} at 900 °C [24] and assuming a diffusion time of $t = 1$ s (the maximum duration for withdrawal of the sample from the furnace and quenching it in cold water), the estimated mean diffusion length of W in γ is calculated to be 3.4 nm. This is in good agreement with the measured width of the W depleted zone observed for the water-quenched sample (~3 nm, see Fig. 4b).

In summary, one can conclude that depletion and segregation of W and Al at the γ/γ' phase boundaries are due to kinetic effects only. They should quickly disappear at operating temperatures (typically not far from the aging temperature for superalloys) due to fast diffusion and hence should be irrelevant to creep properties. The lattice misfit can be derived from the bulk lattice parameters of γ and γ' phases without consideration of such local concentration effects.

Table 2
Average compositions of γ' phase in the ternary alloy measured by APT in laser and voltage modes (in at.%) $\pm 2\sigma$ confidence intervals due to the finite number of ions in the analyzed volumes are given.

APT mode	Co	Al	W
Laser	76.6 ± 0.1	9.4 ± 0.1	14.0 ± 0.1
Voltage	74.7 ± 0.2	10.3 ± 0.2	15.0 ± 0.2

3.5. Hardness of γ and γ'

Recent studies have demonstrated that a higher fraction of γ' results in enhanced creep resistance of both single-crystalline [25] and polycrystalline Co-based superalloys [4]. However, not only the γ' volume fraction but also the γ' strength and its resistance against shearing strongly influence the high-temperature performance of these alloys [26]. Local nanoindentation tests were conducted on individual γ' particles and γ channels. AFM images showing nanoindents and two typical load–displacement curves of the indented γ and γ' phases after applying a maximum load of 150 and 250 μN, respectively, are shown in Fig. 5.

The load–displacement curves in both phases show pop-ins which mark the transition from elastic to plastic deformation and which are an indication of proper sample preparation [27]. The similarity between the curves prior to the pop-in indicates that the elastic properties of the phases are only slightly different, which is also reflected in the average reduced modulus of 215 and 222 GPa for γ and

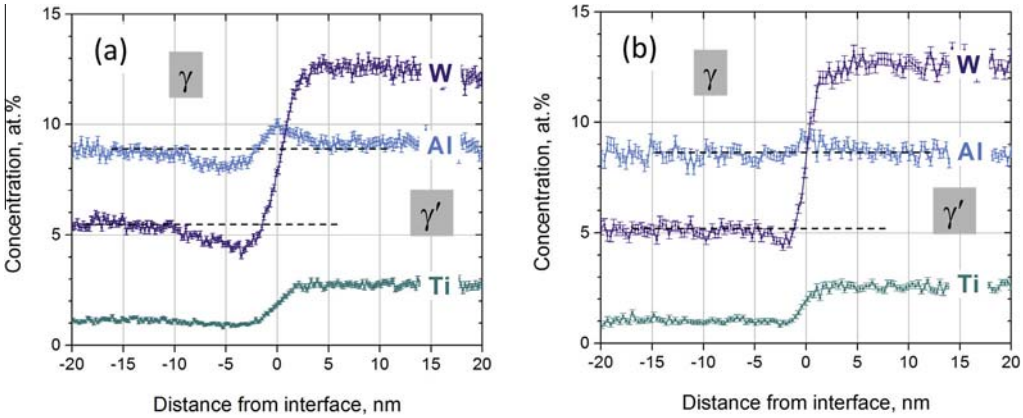

Fig. 4. Elemental concentration profiles for the +2Ti alloy: (a) air-cooled and (b) quenched after aging. Dashed lines show bulk concentrations of corresponding elements in γ matrix.

γ', calculated from the unloading parts of the load–displacement curves of all alloys. This leads to an average Young's modulus of 242 and 252 GPa for γ and γ', respectively, using a Young's modulus of 1141 GPa and a Poisson's ratio of 0.07 for the diamond indenter and a Poisson's ratio of 0.3 for the γ and γ' phase [16]. The Young's modulus of the γ' phase is in good agreement with literature data from Tanaka et al., who reported an experimentally determined polycrystalline Young's modulus of 260 GPa for $Co_3(Al, W)$ [28]. Obviously, the γ phase is elastically softer than the γ' phase; however, quantitative investigations on the alloying effects on the Young's modulus are not performed and discussed here. The cube-corner tip is not ideal for measuring the elastic properties and the phases could influence each other as the elastically deformed volume is bigger than the γ channel width or precipitate size.

Comparing the indents in Fig. 5, it can be seen that at higher loads of 250 μN the size of the indents is in the range of the precipitate size, while at lower loads of 150 μN the indents are much smaller and the indentation depth is only between 20 and 30 nm. In order to investigate whether the plastic zone is small enough and the hardness of γ and γ' is not affected by the other phase, the contact radii of the indents need to be considered. Durst et al. [29] have shown that the influence of the surrounding soft matrix on the properties of particles is 10% when the contact radius reaches 70% of the particle radius and becomes negligible

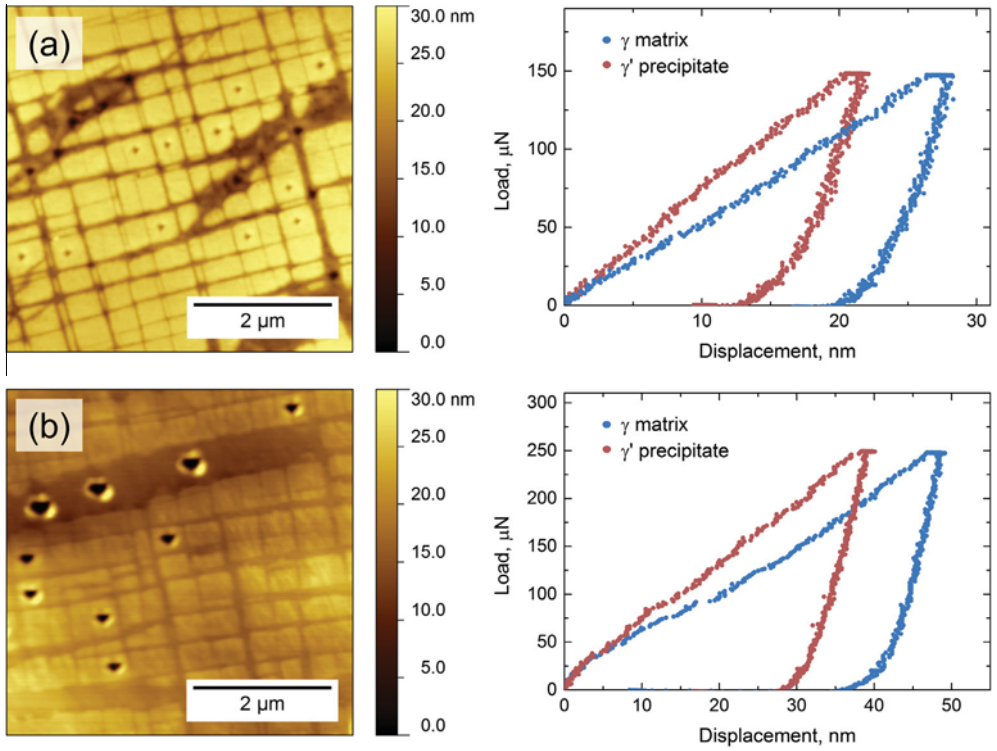

Fig. 5. (a) AFM images showing nanoindents of the alloy +2Ta and corresponding load–displacement curves of indented γ and γ' phases after applying a maximum indentation load of (a) 150 μN and (b) 250 μN.

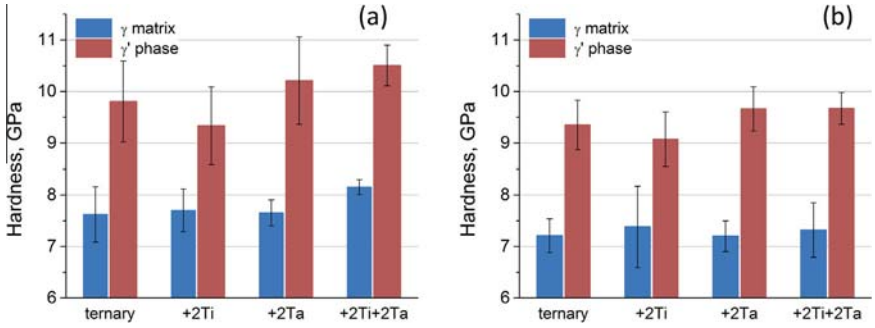

Fig. 6. Hardness of γ and γ' phases of the alloys calculated from nanoindentation measurements with a maximum applied load of (a) 150 μN and (b) 250 μN.

only at contact radii below 55%. In the case of the higher maximum load of 250 μN, contact radii of ~90 nm have been determined. This corresponds to 68% of the precipitate radius for the ternary alloy with the smallest median precipitate size of 265 nm. Although large precipitates have been selected for indentation tests, an influence from the surrounding matrix could not be ruled out completely for indents with 250 μN load. Therefore, indents with an even lower maximum load of 150 μN have also been performed. At this load the influence of the surrounding γ phase can be neglected as the contact radii of 70 nm reach 53% of the precipitate radii at the most. The average hardness of the γ and γ' phases, as determined from averaging over at least eight indentations per phase after applying a maximum load of 150 and 250 μN, respectively, is given in Fig. 6. The resulting hardness is slightly higher when a lower maximum load is used due to the indentation size effect [30], but the trends are very similar. This shows that the measured hardness of the γ and γ' phases is not significantly influenced by the γ/γ' interface or the surrounding phase. The hardness of the γ phase does not change when adding 2 at.% Ta and increases only slightly with additions of 2 at.% Ti, which reflects the partitioning behavior of Ta and Ti. In contrast, the hardness of the γ' phase increases notably when Ta is added to the alloy. Evidently, Ta is not only a very efficient strengthening element of Ni_3Al in Ni-base superalloys, as known from literature [31,32], but also of $Co_3(Al, W)$ in Co-base superalloys. Small additions of Ta (~2 at.%) are reported to enhance the strength of Co–Al–W, especially at temperatures above 700 °C [3,7]. Applying ab initio density functional theory (DFT), Mottura et al. [33] calculated that substitution of W by Ta in the $Co_3(Al, W)$ lattice leads to a significant increase in the superlattice intrinsic stacking fault energy. As a result, the stress required for shearing γ'-$Co_3(Al, W)$ particles by a/3⟨1 1 2⟩ superpartial dislocations is substantially increased. This effect, together with the increased volume fraction of γ', is considered to be the cause of the increase in strength upon alloying with Ta. In the present study, we directly linked the enhanced hardness of γ' particles in the Co–Al–Ta alloy to the substitution of W by Ta in the B-sublattice of γ'.

Furthermore, W substitution by Ta can affect the elastic properties of the γ' phase. It was previously reported that the $Co_3(Al, W)$ phase has higher elastic moduli than Ni_3Al [34]. The effect of Ta (Ti) on the atomic bonding, and hence the elastic moduli and strength of the γ' $Co_3(Al, W)$ phase, remains to be studied using ab initio DFT calculations. Surprisingly, Ti does not show such a strong hardening effect on the γ' phase as Ta. Moreover, additions of Ti are even found to decrease the γ' hardness when compared to the ternary alloy. This observation can be explained by the measured concentrations of strengthening elements in the γ' phase (see Table 1): Ti additions lead to a decrease in W concentration in γ'. Hence, we conclude that Ti is a weaker strengthener than W and especially Ta, being similar to the strengthening effect of these elements in Ni-based alloys [31,32] and thus cannot compensate for the decreased concentration of W.

4. Conclusions

1. W, Ti and Ta partition to the γ' phase in aged Co-based superalloys. The partitioning coefficients depend on alloy composition. Al shows very low partitioning in ternary Co–Al–W alloys, which further decreases upon adding Ti or Ta. The γ' volume fraction increases considerably in the alloys containing Ti and/or Ta.
2. Based on the γ' composition we conclude that Al, W, Ti and Ta occupy the B sublattice of the γ' phase (A_3B compound with $L1_2$-type of ordering). However, no direct experimental proof is currently available.
3. Enrichment and depletion zones of Al and W have been found at the γ/γ' interfaces in the aged alloys. These local compositional effects arise during slow cooling from aging temperatures and are substantially suppressed by water-quenching. They are expected to be absent at typical operation temperatures of superalloys and hence irrelevant to the creep properties.
4. The hardness of the γ channels remains nearly constant in all alloys. The hardness of the γ' phase increases in Ta-containing alloys, showing similarity to Ni-base superalloys and being in agreement with recent ab initio

calculations of the stacking fault energy in Ta-doped Co_3(Al, W). The hardening effect of Ti is weaker than that of W and especially Ta.

Acknowledgments

The work was supported by the Deutsche Forschungsgemeinschaft (DFG) through Projects A4 and B3 of the Collaborative Research Center SFB Transregio/103 "From Atoms to Turbine Blades—A Scientific Approach for Developing the Next Generation of Single Crystal Superalloys".

References

[1] Sato J, Omori T, Oikawa K, Ohnuma I, Kainuma R, Ishida K. Science 2006;312:90.
[2] Tsunekane M, Suzuki A, Pollock TM. Intermetallics 2011;19:636.
[3] Pollock TM, Dibbern J, Tsunekane M, Zhu J, Suzuki A. JOM 2010;62:58.
[4] Bauer A, Neumeier S, Pyczak F, Singer RF, Göken M. Mater Sci Eng, A 2012;550:333.
[5] Kobayashi S, Tsukamoto Y, Takasugi T. Intermetallics 2012;31:94.
[6] Omori T, Oikawa K, Sato J, Ohnuma I, Kattner UR, Kainuma R, et al. Intermetallics 2013;32:274.
[7] Suzuki A, Pollock TM. Acta Mater 2008;56:1288.
[8] Kobayashi S, Tsukamoto Y, Takasugi T. Intermetallics 2011;19:1908.
[9] Meher S, Yan HY, Nag S, Dye D, Banerjee R. Scripta Mater 2012;67:850.
[10] Meher S, Nag S, Tiley J, Goel A, Banerjee R. Acta Mater 2013;61:4266.
[11] Bocchini PJ, Lass EA, Moon K-W, Williams ME, Campbell CE, Kattner UR, et al. Scripta Mater 2013;68:563.
[12] Yan HY, Vorontsov VA, Dye D. Intermetallics 2014;48:44.
[13] Göken M, Kempf M. Acta Mater 1999;47:1043.
[14] Neumeier S, Pyczak F, Göken M. Phil Mag 2011;91:4187.
[15] Thompson K, Lawrence D, Larson DJ, Olson JD, Kelly TF, Gorman B. Ultramicroscopy 2007;107:131.
[16] Oliver WC, Pharr GM. J Mater Res 1992;7:1564.
[17] Wanderka N, Glatzel U. Mater Sci Eng, A 1995;203:69.
[18] Amouyal Y, Mao Z, Booth-Morrison C, Seidman DN. Appl Phys Lett 2009;94:041917.
[19] Saal JE, Wolverton C. Acta Mater 2013;61:2330.
[20] Yamaguchi Y, Takahashi J, Kawakami K. Ultramicroscopy 2009;109:541.
[21] Costa GD, Wang H, Duguay S, Bostel A, Blavette D, Deconihout B. Rev Sci Instrum 2012;83:123709.
[22] Hudson D, Smith GDW, Gault B. Ultramicroscopy 2011;111:480.
[23] Okamoto H. J Phase Equilib Diffus 2008;29:119.
[24] Cui YW, Xu G, Kato R, Lu X-G, Kainuma R, Ishida K. Metall Mater Trans A 2013;44:1621.
[25] Titus MS, Suzuki A, Pollock TM. Scripta Mater 2012;66:574.
[26] Carroll LJ, Feng Q, Pollock TM. Metall Mater Trans A 2008;39:1290.
[27] Göken M, Kempf M. Z Metallkd 2001;92:7.
[28] Tanaka K, Ohashi T, Kishida K, Inui H. Appl Phys Lett 2007;91:181907.
[29] Durst K, Göken M, Vehoff H. J Mater Res 2004;19:85.
[30] Nix WD, Gao H. J Mech Phys Solids 1998;46:411.
[31] Mishima Y, Ochiai S, Hamao N, Yodogawa M, Suzuki T. Trans Jpn Inst Met 1986;27:648.
[32] Mishima Y, Ochiai S, Hamao N, Yodogawa M, Suzuki T. Trans Jpn Inst Met 1986;27:656.
[33] Mottura A, Janotti A, Pollock TM. Intermetallics 2012;28:138.
[34] Yao Q, Xing H, Sun J. Appl Phys Lett 2006;89:161906.